ARL-TR-9620 • Dec 2022

DEVCOM ARMY RESEARCH LABORATORY

Dynamic Inversion with Adaptive Augmentation for a High-Speed Guided Projectile

by Tristan D Griffith, John Zelina, Joshua T Bryson, and Benjamin C Gruenwald

NOTICES

Disclaimers

The findings in this report are not to be construed as an official Department of the Army position unless so designated by other authorized documents.

Citation of manufacturer's or trade names does not constitute an official endorsement or approval of the use thereof.

Destroy this report when it is no longer needed. Do not return it to the originator.

ARL-TR-9620 ● DEC 2022

Dynamic Inversion with Adaptive Augmentation for a High-Speed Guided Projectile

Tristan D Griffith
Texas A&M University

John Zelina
Embry-Riddle Aeronautical University

Joshua T Bryson and Benjamin C Gruenwald
DEVCOM Army Research Laboratory

REPORT DOCUMENTATION PAGE

Form Approved
OMB No. 0704-0188

PLEASE DO NOT RETURN YOUR FORM TO THE ABOVE ADDRESS.

1. REPORT DATE *(DD-MM-YYYY)*	2. REPORT TYPE	3. DATES COVERED (From - To)
December 2022	Technical Report	1 June–16 September 2022

4. TITLE AND SUBTITLE
Dynamic Inversion with Adaptive Augmentation for a High-Speed Guided Projectile

5a. CONTRACT NUMBER

5b. GRANT NUMBER

5c. PROGRAM ELEMENT NUMBER

6. AUTHOR(S)
Tristan D Griffith, John Zelina, Joshua T Bryson, and Benjamin C Gruenwald

5d. PROJECT NUMBER

5e. TASK NUMBER

5f. WORK UNIT NUMBER

7. PERFORMING ORGANIZATION NAME(S) AND ADDRESS(ES)
DEVCOM Army Research Laboratory
ATTN: FCDD-RLA-WD
Aberdeen Proving Ground, MD 21005

8. PERFORMING ORGANIZATION REPORT NUMBER
ARL-TR-9620

9. SPONSORING/MONITORING AGENCY NAME(S) AND ADDRESS(ES)

10. SPONSOR/MONITOR'S ACRONYM(S)

11. SPONSOR/MONITOR'S REPORT NUMBER(S)

12. DISTRIBUTION/AVAILABILITY STATEMENT
Approved for public release; distribution is unlimited.

13. SUPPLEMENTARY NOTES
primary author's email: <joshua.t.bryson.civ@army.mil>.
ORCID: Joshua Bryson, 0000-0002-0753-6823; Benjamin Gruenwald, 0000-0003-3968-5070

14. ABSTRACT
Dynamic inversion control schemes offer a systematic approach to flight control design when the relevant plant dynamics are well characterized. This work presents a dynamic inversion scheme for the autopilot of a high-speed projectile. The relevant aerodynamic coefficients for the projectile's short period dynamics are well characterized and used here to develop a scheduled linear dynamic inversion controller. An adaptive modification is included to correct the aerodynamic coefficients in the outer loop of the control architecture where the greatest sensitivity to parametric uncertainty is found. The resultant approach is exercised through a series of nonlinear simulations and shows graceful degradation in the presence of a variety of uncertainties.

15. SUBJECT TERMS flight control, dynamic inversion, adaptive control, guided projectile, high-speed projectile, tail-control, Weapons Sciences

16. SECURITY CLASSIFICATION OF:			17. LIMITATION OF ABSTRACT	18. NUMBER OF PAGES	19a. NAME OF RESPONSIBLE PERSON
a. REPORT	b. ABSTRACT	c. THIS PAGE			Joshua T Bryson
Unclassified	Unclassified	Unclassified	UU	36	19b. TELEPHONE NUMBER (Include area code) 410-306-1939

Contents

List of Figures

List of Tables

1. Introduction

In the early stages of a new munition design process, it is desirable to quickly update the controller as the aerodynamics and mass properties evolve. This allows for timely evaluation of closed-loop maneuverability and system performance metrics to provide input for the overall system development, including the lifting and stabilizing surface sizing, control surface properties, actuation system requirements, and sensor specifications. This research explores methodologies to rapidly design effective flight control for high-speed guided munitions to enable desired operation across an expanded flight envelope.

Previous work investigated the use of a gain scheduled three-loop autopilot for a tail-controlled, high-speed projectile.[1,2] This work was focused on streamlining and automating the gain scheduling process and has resulted in a significant improvement to the flight control design time line compared to the legacy approach. This work continues our investigation into alternative control strategies for tail-controlled, high-speed projectiles by exploring the application of dynamic inversion control as a systematic, physically derived alternative to gain scheduling. We particularly wish to explore the hypothesis here that dynamic inversion controllers offer straightforward design and implementation for flight dynamics that are well characterized across the flight envelope, acting as a baseline, bolt-on architecture for new projectiles.

Dynamic inversion controllers have been widely used in a variety of applications, including flight control.[3,4] Crucially, tail-controlled projectiles, such as the one considered here, often exhibit nonminimum phase dynamics in the desired control variable. Under dynamic inversion, the plant zeros become the plant poles.[5] Lee et al.[5] treat this issue with a modified feedback architecture, while Kutluay and Yavrucuk[6] consider an additional loop to mitigate the unstable transmission zero. Robustness has been addressed using a time scale separation scheme[7] or with adaptive augmentation.[8]

Before discussing the design of the dynamic inversion controller applied in this work, we first present the airframe dynamics for the considered projectile.

2. Projectile Flight Dynamics

In this section, we provide a brief overview of the nonlinear flight dynamics for a generic tail-controlled projectile. More details can be found in Bryson and Gruenwald.[2] We begin by noting the relevant reference frames and coordinate systems needed to describe the position and orientation of the projectile. As shown in Fig. 1, the earth reference frame is used as the inertial frame located at the launch location with the x-axis pointing toward the target and the body-fixed reference frame is fixed at the center-of-gravity (CG) location on the body of the projectile.

The orientation of the body-fixed frame can be given with respect to the fixed earth reference frame using a ZYX Euler sequence of rotations, where the three Euler angles for roll, pitch, and yaw, are given by ϕ, θ, and ψ, respectively. Using this transformation, the kinematic equations for translational velocity can be given as

$$\begin{bmatrix} \dot{x} \\ \dot{y} \\ \dot{z} \end{bmatrix} = \begin{bmatrix} \mathrm{c}_\theta \mathrm{c}_\psi & \mathrm{s}_\phi \mathrm{s}_\theta \mathrm{c}_\psi - \mathrm{c}_\phi \mathrm{s}_\psi & \mathrm{c}_\phi \mathrm{s}_\theta \mathrm{c}_\psi + \mathrm{s}_\phi \mathrm{s}_\psi \\ \mathrm{c}_\theta \mathrm{s}_\psi & \mathrm{s}_\phi \mathrm{s}_\theta \mathrm{s}_\psi + \mathrm{c}_\phi \mathrm{c}_\psi & \mathrm{c}_\phi \mathrm{s}_\theta \mathrm{s}_\psi - \mathrm{s}_\phi \mathrm{c}_\psi \\ -\mathrm{s}_\theta & \mathrm{s}_\phi \mathrm{c}_\theta & \mathrm{c}_\phi \mathrm{c}_\theta \end{bmatrix} \begin{bmatrix} u \\ v \\ w \end{bmatrix}, \tag{1}$$

where $\mathrm{s}_\phi = \sin(\phi)$, $\mathrm{c}_\phi = \cos(\phi)$, and so forth, the states $[x, y, z]^{\mathrm{T}}$ are the CG positions relative to the earth inertial frame, and $[u, v, w]^{\mathrm{T}}$ are the body-fixed translational velocities.

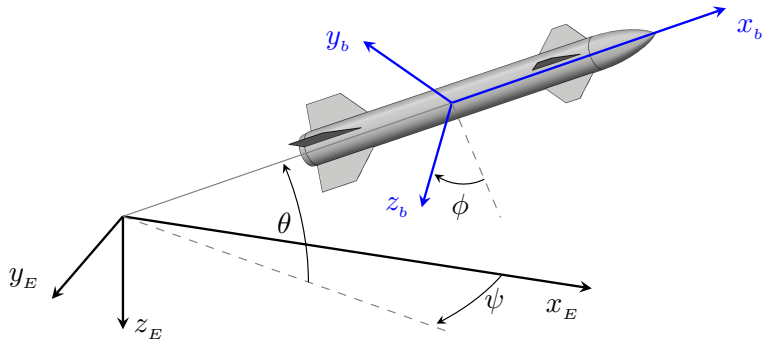

Fig. 1 Illustration of a generic projectile with a body-fixed frame relative to an earth reference frame (inertial frame)

The dynamics of the Euler angles can be described by the body-fixed angular rates

as the following kinematic equations

$$\begin{bmatrix} \dot{\phi} \\ \dot{\theta} \\ \dot{\psi} \end{bmatrix} = \begin{bmatrix} 1 & \mathrm{s}_\phi \mathrm{t}_\theta & \mathrm{c}_\phi \mathrm{t}_\theta \\ 0 & \mathrm{c}_\phi & -\mathrm{s}_\phi \\ 0 & \mathrm{s}_\phi / \mathrm{c}_\theta & \mathrm{c}_\phi / \mathrm{c}_\theta \end{bmatrix} \begin{bmatrix} p \\ q \\ r \end{bmatrix}, \tag{2}$$

where $[p, q, r]^{\mathrm{T}}$ are the body-fixed angular rates acting in the roll, pitch, and yaw planes, respectively, and $\mathrm{t}_\theta = \tan(\theta)$.

The projectile flight dynamics are based on the standard rigid body 6-degree-of-freedom equations of motion. The three translational degrees of freedom are governed by Newton's second law and described by the body-fixed translational velocities given by

$$\begin{bmatrix} \dot{u} \\ \dot{v} \\ \dot{w} \end{bmatrix} = \frac{1}{m} \begin{bmatrix} F_X - mg\mathrm{s}_\theta \\ F_Y + mg\mathrm{s}_\phi \mathrm{c}_\theta \\ F_Z + mg\mathrm{c}_\phi \mathrm{c}_\theta \end{bmatrix} - \begin{bmatrix} 0 & -r & q \\ r & 0 & -p \\ -q & p & 0 \end{bmatrix} \begin{bmatrix} u \\ v \\ w \end{bmatrix}. \tag{3}$$

Here m is the mass of the projectile, g is the gravitational acceleration, and F_X, F_Y, and F_Z are the aerodynamic forces acting on the projectile body in the x, y, and z direction, respectively. The three rotational degrees of freedom are governed by Euler's law and described by the body-fixed angular rates given by

$$\begin{bmatrix} \dot{p} \\ \dot{q} \\ \dot{r} \end{bmatrix} = \begin{bmatrix} I_x^{-1} & 0 & 0 \\ 0 & I_y^{-1} & 0 \\ 0 & 0 & I_z^{-1} \end{bmatrix} \begin{bmatrix} M_l \\ M_m \\ M_n \end{bmatrix} + \begin{bmatrix} I_x^{-1}(I_y - I_z)qr \\ I_y^{-1}(I_z - I_x)pr \\ I_z^{-1}(I_x - I_y)pq \end{bmatrix}, \tag{4}$$

where I_x, I_y, and I_z are the components of inertia around the x, y, and z axes, and M_l, M_m, and M_n are the external moment components resulting from the aerodynamic moments. The inertia matrix is considered to be diagonal with no cross-coupling owing to the symmetric nature of the considered projectile bodies.

Now we introduce the wind reference frame, depicted in Fig. 2, which is defined by the instantaneous orientation of the relative wind velocity vector, denoted as $\vec{V} \equiv \vec{V}_{CG/E}$, with respect to the body-fixed frame. The relationship between the wind frame and the body-fixed frame is made through the aerodynamic angles:

angle of attack, α, and angle of sideslip, β. In addition, the airspeed of the projectile is given by the magnitude of the velocity vector $\vec{V}$ and can be written as

$$V = \sqrt{u^2 + v^2 + w^2}, \tag{5}$$

and the aerodynamic angles can be written in terms of the body-fixed component velocities as

$$\alpha = \arctan\left(\frac{w}{u}\right), \tag{6}$$

$$\beta = \arcsin\left(\frac{v}{V}\right). \tag{7}$$

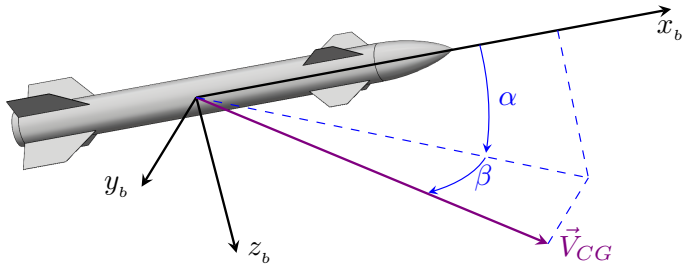

Fig. 2 Wind reference frame relative to the body-fixed reference frame. Angle of attack and angle of sideslip relate to the projectile's CG velocity vector.

With the full 6-degree-of-freedom equations of motion defined, we now note the common practice of linearizing and decoupling the dynamics into the longitudinal and lateral-directional modes. For the purpose of this report, we consider the short-period mode of the longitudinal dynamics. The short-period mode is described by the dynamics of angle of attack α and pitch rate q. Using Eqs. 3 and 4, along with the appropriate forces and moments, and Eq. 6, the short-period dynamics can be written as

$$\begin{bmatrix} \dot{\alpha} \\ \dot{q} \end{bmatrix} = \begin{bmatrix} \frac{Z_\alpha}{V} & 1 \\ M_\alpha + M_{\dot{\alpha}}\frac{Z_\alpha}{V} & M_q + M_{\dot{\alpha}} \end{bmatrix} \begin{bmatrix} \alpha \\ q \end{bmatrix} + \begin{bmatrix} \frac{Z_{\delta_q}}{V} \\ M_{\delta_q} + M_{\dot{\alpha}}\frac{Z_{\delta_q}}{V} \end{bmatrix} \delta_q. \tag{8}$$

Here, δ_q is the control input for pitch motion, and the terms Z_α, M_α, $M_{\dot{\alpha}}$, M_q, Z_{δ_q}, and M_{δ_q} are dimensional derivatives and given in Table 1 where $Q = \frac{1}{2}\rho V^2$ is the dynamic pressure (ρ being the air density), $S = \frac{\pi}{4}D^2$ is the aerodynamic reference area, and D is the projectile diameter. The stability and derivative coefficients given

by C_{Z_α}, C_{m_α}, $C_{m_{\dot{\alpha}}}$, C_{m_q}, $C_{Z_{\delta_q}}$, and $C_{m_{\delta_q}}$ are obtained from aerodynamic modeling of the forces and moments on the projectile.

Table 1 Dimensional derivative terms

$Z_\alpha = \frac{QS}{m} C_{Z_\alpha}$	$Z_\delta = \frac{QS}{m} C_{Z_{\delta_q}}$
$M_\alpha = \frac{QSD}{I_y} C_{m_\alpha}$	$M_{\dot{\alpha}} = \frac{QSD}{I_y} \frac{D}{2V} C_{m_{\dot{\alpha}}}$
$M_q = \frac{QSD}{I_y} \frac{D}{2V} C_{m_q}$	$M_\delta = \frac{QSD}{I_y} C_{m_{\delta_q}}$

Since the control objective will be to follow a desired acceleration command, we note here that the projectile's specific vertical acceleration $A_z = -F_Z/m$ can be written as

$$A_z = \begin{bmatrix} -Z_\alpha & 0 \end{bmatrix} \begin{bmatrix} \alpha \\ q \end{bmatrix} + \begin{bmatrix} -Z_{\delta_q} \end{bmatrix} \delta_q, \tag{9}$$

where the negative sign is used by convention so a positive angle of attack supplies a positive vertical acceleration.

3. Dynamic Inversion Control

3.1 Brief Overview of Dynamic Inversion Control for Flight Control

Consider the class of systems described by the coupled ordinary differential equations

$$\begin{aligned} \dot{x} &= Ax + Bu \\ y &= Cx + Du. \end{aligned} \tag{10}$$

Here, $x(t) \in \boldsymbol{X}$ is the state vector, $u(t) \in \boldsymbol{U}$ is an input, and the output is $y(t) \in \boldsymbol{Y}$. The state vector is an *n*-dimensional vector evolving in $\boldsymbol{X} \equiv \mathbb{C}^n$. Accordingly, the inputs evolve in the *m*-dimensional space $\boldsymbol{U} \equiv \mathbb{C}^m$ and the outputs in *p*-dimensional space $\boldsymbol{Y} \equiv \mathbb{C}^p$.

The aim of dynamic inversion generally is to include the inverse of the system dynamics in the control so that the closed loop properties of the dynamics may be set according to desired performance characteristics. Conceptually, the system

dynamics must appear in some form in the control vector u. If the matrix D is nonzero and has a right inverse $D^\dagger \ni DD^\dagger = I$, it can be seen that setting the control input to

$$u = D^\dagger(v - Cx), \tag{11}$$

yields the closed loop dynamics

$$\dot{x} = Ax + B(D^\dagger(v - Cx)) \tag{12a}$$
$$= (A - BD^\dagger C)x + BD^\dagger v \tag{12b}$$

with the output

$$y = Cx + DD^\dagger(v - Cx) \tag{13a}$$
$$= v. \tag{13b}$$

Accordingly, the system is decoupled ($y_i = v_i$) and the output can be explicitly set with the "virtual" control vector v.

Of course, there may be no feedthrough matrix D. In such cases, derivatives of the output y until there is a feedthrough term on a given output derivative $y^{(d)}$

$$y^{(d)} = \begin{bmatrix} y_1^{d_1} \\ y_2^{d_2} \\ \vdots \\ y_r^{d_r} \end{bmatrix} = Fx + Eu \tag{14}$$

where F and E are matrices generated by the relevant Lie derivative

$$F_i = \begin{cases} C_i & d_i = 0 \\ C_i A^{d_i} & d_i \geq 1 \end{cases}, \; E_i = \begin{cases} D_i & d_i = 0 \\ C_i A^{d_i - 1} B & d_i \geq 1. \end{cases} \tag{15}$$

The r^{th} derivative resulting in a nonzero E is the *relative degree* of the system. Dynamic inversion controllers are especially favorable for flight control because the relative degree of the system tends to be ≤ 1. The virtual control v now prescribes the desired behavior of the output derivative $v = y^{(d)}_{\text{desired}}$. A system with relative

degree r has the closed loop behavior

$$\dot{x} = (A - BE_r^\dagger F)x + BE_r^\dagger v \tag{16a}$$

$$y^{(d)} = v \tag{16b}$$

and the closed loop output dynamics are once again decoupled and may be prescribed according to v.

Interested readers should explore additional literature[5,9–12] for a broader theoretical treatment of both linear and nonlinear dynamic inversion approaches for flight control. It suffices to say for the control of this tail-controlled projectile, linear dynamic inversion controllers of low relative order are sufficient to set the closed loop dynamics across the flight envelope. With this brief overview complete, we proceed to synthesizing the dynamic inversion controller for the example projectile.

3.2 Dynamic Inversion Approach for Projectile Longitudinal Dynamics

Dynamic inversion control architectures are amenable to multivariate dynamics,[5,13] such as those in Eq. 8. However, a dynamic inversion approach is *not* appropriate here because the A_z dynamics have an unstable transmission zero throughout the flight envelope and are therefore nonminimum phase. Because the open loop zeros become closed loop poles under dynamic inversion,[5] unmodified dynamic inversion controllers for the A_z loop will destabilize the system dynamics, so we cannot simply invert the A_z dynamics to generate a deflection command δ_q. Accordingly, we choose to use a time scale separation scheme here. Time scale separation approaches are desirable because they allow for the design of low-order controllers, simplify the control scheme conceptually, and have been shown to be more robust than multivariate controllers that do not use time scale separation.[7] It is typical to consider the actuator dynamics of a projectile as the fastest for time scale separation purposes.[12] The body angular rates are the next fastest, followed by the angle of attack or acceleration rates.[14] This also allows for the treatment of the nonminimum phase dynamics.

It is worth noting that this approach uses simplified, linear equations for the nonlinear projectile dynamics. For aerospace systems, much effort is typically invested in characterizing the dynamics across various conditions,[15–17] so these nonlinear dynamics are usually understood and incorporated into the nonlinear model. Given

sufficient sample points within a discretized flight envelope, the interpolated family of linear models is representative of the nonlinear behavior across the flight envelope. Accordingly, our dynamic inversion controller will interpolate the aerodynamic coefficients across the envelope to handle nonlinear behavior. This approach is well established in the literature as dynamic inversion controllers are especially effective when the system dynamics are well characterized.[14]

3.2.1 Fast Inner Loop

Here, we consider the q dynamics in the "fast" inner loop. The inner loop dynamics extracted from Eq. 8 are

$$\dot{q} = \left(M_\alpha + M_{\dot{\alpha}} \frac{Z_\alpha}{V} \right) \alpha + (M_q + M_{\dot{\alpha}}) q + \left(M_{\delta_q} + M_{\dot{\alpha}} \frac{Z_{\delta_q}}{V} \right) \delta_q. \tag{17}$$

Dropping small terms divided by the airspeed V and denoting $M_{\tilde{q}} \equiv M_q + M_{\dot{\alpha}}$ as the entire damping sum yields

$$\dot{q} = M_\alpha \alpha + M_{\tilde{q}} q + M_{\delta_q} \delta_q. \tag{18}$$

The appropriate dynamic inversion controller for the dynamics in Eq. 18 is then

$$\delta_q = M_{\delta_q}^{-1} \left(v_q - M_\alpha \alpha - M_{\tilde{q}} q \right). \tag{19}$$

Equation 19 does not account for actuator dynamics, which are known to degrade control outcomes by interfering with the ability of the flight controller to access the plant dynamics.[18] Here, a first-order model is used to account for the effect of actuator dynamics within the control design

$$\dot{\delta}_q = \omega_n (\delta_\mathrm{d} - \delta_q) \tag{20}$$

where the deflection command δ_d is related to the control surface deflection δ_q through the actuator bandwidth ω_n. Solving for δ_q in Eq. 20 yields

$$\delta_q = \delta_\mathrm{d} - \frac{\dot{\delta}_q}{\omega_n}. \tag{21}$$

If we substitute Eq. 21 into Eq. 19, we obtain

$$\delta_\mathrm{d} = M_{\delta_q}^{-1} (v_q - M_\alpha \alpha - M_{\tilde{q}} q) + \frac{\dot{\delta}_q}{\omega_n}. \tag{22}$$

Equation 22 yields a control scheme that accounts for actuator bandwidth. In practice, the actuator rate $\dot{\delta}_q$ may not be available as a measurement, so we will use an internal model of the actuator of the form in Eq. 20 to feedback $\dot{\delta}_q$. Generally, actuator dynamics in dynamic inversion controllers may be accounted for by taking further derivatives of the output before substituting the actuator dynamics and solving for the appropriate controller using plant states.[12,19] By using an internal model of the first-order actuator here, we simplify the controller synthesis while still accounting for some of the actuator effects.

Notice, inserting the actuator approximation Eq. 21 into Eq. 18 yields

$$\dot{q} = M_\alpha \alpha + M_{\tilde{q}} q + M_{\delta_q}(\delta_\mathrm{d} - \frac{\dot{\delta}_q}{\omega_n}) \tag{23}$$

and we may now insert the dynamic inversion controller in Eq. 22 into Eq. 23 to realize

$$\dot{q} = M_\alpha \alpha + M_{\tilde{q}} q + M_{\delta_q} \left(M_{\delta_q}^{-1}(v_q - M_\alpha \alpha - M_{\tilde{q}} q) + \frac{\dot{\delta}_q}{\omega_n} - \frac{\dot{\delta}_q}{\omega_n} \right) \tag{24a}$$

$$= M_\alpha \alpha + M_{\tilde{q}} q + (v_q - M_\alpha \alpha - M_{\tilde{q}} q) \tag{24b}$$

$$= M_\alpha \alpha - M_\alpha \alpha + M_{\tilde{q}} q - M_{\tilde{q}} q + v_q \tag{24c}$$

$$= v_q. \tag{24d}$$

Of course, the ability to reduce the dynamics to Eq. 24d is sensitive to how accurate the aerodynamic coefficients and actuator models are for a given point in the flight envelope. Now, the question is how to assign the control input v. Following Kutluay and Yavrucuk[6] and Tipàn et al.,[3] state feedback is used to set the desired closed loop bandwidth. One of the advantages of the dynamic inversion approach here is the ability to carefully set closed loop properties in order to meet design requirements.[20] Accordingly,

$$v_q = \omega_q \underbrace{(q_\mathrm{d} - q)}_{e_q} \tag{25a}$$

$$= \omega_q e_q \tag{25b}$$

where ω_q is the desired closed loop bandwidth for the q loop and q_d is the desired

angular rate from the α loop. The closed loop system dynamics are then simply

$$\dot{q} = \omega_q e_q. \tag{26}$$

3.2.2 Slow Outer Loop

The α dynamics have a lower relative control effectiveness when compared to the q dynamics and so they form the slow outer loop of this time separation scheme. The α dynamics parsed from Eq. 8 take the form

$$\dot{\alpha} = \frac{Z_\alpha}{V}\alpha + q + \frac{Z_{\delta_q}}{V}\delta_q. \tag{27}$$

In this application Z_{δ_q} is dropped and treated as a disturbance since $Z_\alpha >> Z_{\delta_q}$

$$\dot{\alpha} = \frac{Z_\alpha}{V}\alpha + q. \tag{28}$$

The dynamic inversion controller for this loop is

$$q_\mathrm{d} = v_\alpha - \frac{Z_\alpha}{V}\alpha, \tag{29}$$

which substituted into Eq. 28 yields

$$\dot{\alpha} = \frac{Z_\alpha}{V}\alpha + v_\alpha - \frac{Z_\alpha}{V}\alpha \tag{30a}$$

$$= v_\alpha. \tag{30b}$$

Following the low-order control design in Eq. 25b, we set the desired v_α as

$$v_\alpha = \omega_\alpha(\alpha_\mathrm{d} - \alpha) \tag{31}$$

where ω_α is the desired closed loop bandwidth for the α loop and α_d is the desired angle of attack from the A_z guidance filter, resulting in the control law

$$q_\mathrm{d} = \omega_\alpha(\alpha_\mathrm{d} - \alpha) - \frac{Z_\alpha}{V}\alpha. \tag{32}$$

3.3 Body Acceleration Loop

In order to track reference commands from the projectile guidance law, an α_{d} command must be generated from the body acceleration A_z dynamics. However, a dynamic inversion approach is *not* appropriate here because the A_z dynamics have an unstable transmission zero throughout the flight envelope and are therefore nonminimum phase. Because the open loop zeros become closed loop poles under dynamic inversion,[5] unmodified dynamic inversion controllers for the A_z loop will destabilize the system dynamics.

3.3.1 Proportional Integral α Command Generator

From Kutluay and Yavrucuk,[6] a physically derived scheme can be implemented. The A_z dynamics from Eq. 9 are

$$A_z = -Z_\alpha \alpha - Z_{\delta_q} \delta_q. \tag{33}$$

As in Eq. 28, Z_{δ_q} is dropped such that

$$-Z_\alpha^{-1} A_z = \alpha \tag{34}$$

yielding a physically "scheduled" gain for converting A_z commands to α commands. Of course, we should not expect this conversion to be perfect, so an integral controller is also included to the reference tracking error

$$\alpha_{\mathrm{d}} = -Z_\alpha^{-1} A_z + K_i \int_0^t (A_z(\tau) - A_{z,\mathrm{d}}(\tau)) d\tau \tag{35a}$$

$$\alpha_{\mathrm{d}} = -Z_\alpha^{-1} A_z + K_i \int_0^t e_{A_z}(\tau) d\tau. \tag{35b}$$

This scheme is represented graphically in Fig. 3. The projectile guidance system delivers a desired body acceleration command $A_{z,\mathrm{d}}$. A desired angle of attack α_{d} is produced by the "α command generator," which utilizes the control law in Eq. 35b. α_{d} is then used as the input to the slow dynamic inversion loop, which controls the α dynamics via the synthesized law in Eq. 32. This slow loop in turn commands the fast dynamic inversion q loop, which ultimately synthesizes a control surface deflection δ_{d} that accounts for first-order actuator dynamics per Eq. 22.

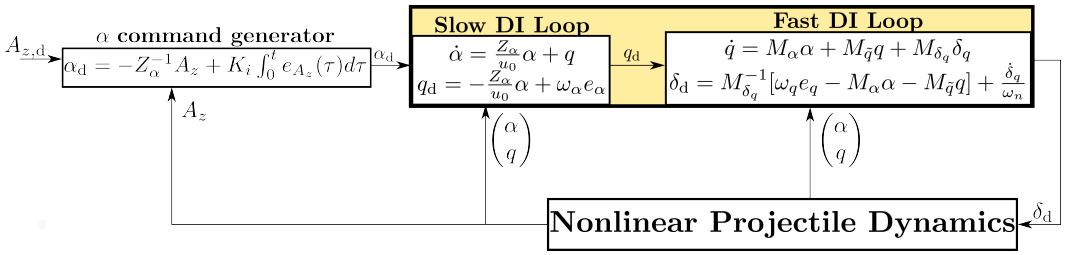

Fig. 3 Dynamic inversion control scheme for the projectile with integral α command generator

3.3.2 Adaptive α Command Generator

Because the α command scheme here is based on a series of simplifications, an adaptive α command generator is introduced because we expect significant sensitivity to parametric uncertainty in Z_α^{-1}. We may consider an adaptive identification scheme to continuously update the proportional term so that the integral error controller in Eq. 35b may not be needed.

Consider the slow dynamic inversion loop, where the plant dynamics are

$$\dot{\alpha} = \omega_\alpha(\alpha_{\mathrm{CMD}} - \alpha) \tag{36a}$$

$$= -\omega_\alpha \alpha - \omega_\alpha Z_\alpha^{-1} A_{z,\mathrm{CMD}}. \tag{36b}$$

Our controller may have the wrong estimate of Z_α^{-1}

$$\dot{\hat{\alpha}} = -\omega_\alpha \hat{\alpha} - \omega_\alpha \bar{Z}_\alpha^{-1} A_{z,\mathrm{CMD}} \tag{37}$$

where $\bar{Z}_\alpha^{-1} \neq Z_\alpha^{-1}$. We wish to implement an adaptive scheme to correct $\bar{Z}_\alpha^{-1}$ online. The adaptive gain law

$$\Delta \dot{Z}_\alpha^{-1} \equiv -e_{A_z} A_{z,\mathrm{CMD}}^* \sigma, \sigma > 0, \tag{38}$$

corrects $\bar{Z}_\alpha^{-1}$ online and is stable under the analysis presented in the Appendix.

This scheme is presented graphically in Fig. 4. This adaptive dynamic inversion controller operates exactly as the scheme in Fig. 3, except for the α-command generator. While the control scheme described here is for the longitudinal dynamics, a similar line of thinking follows for the lateral dynamics.[3] With this technical treatment complete, we turn to implementation details and simulation results.

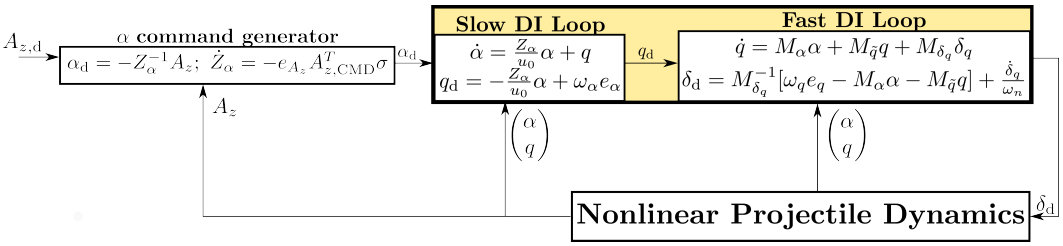

Fig. 4 Dynamic inversion control scheme for the projectile with adaptive α command generator

4. Simulation and Implementation Results

4.1 Controller Implementation

The dynamic inversion controller is designed over a flight envelope defined by

$$\Gamma : \begin{cases} 1.2 \leq \mathcal{M} \leq 3.5 \\ |\alpha| \leq 12^\circ. \end{cases} \tag{39}$$

The flight envelope is discretized into a set of linear operating points and the projectile is trimmed and linearized at each point yielding a set of linear models spanning the flight envelope, according to the form of Eq. 8.

The actuator dynamics for the projectile are assumed to behave as a second-order system

$$\begin{bmatrix} \dot{\delta}_q \\ \ddot{\delta}_q \end{bmatrix} = \begin{bmatrix} 0 & 1 \\ -\omega_n^2 & -2\zeta\omega_n \end{bmatrix} \begin{bmatrix} \delta_q \\ \dot{\delta}_q \end{bmatrix} + \begin{bmatrix} 0 \\ \omega_n^2 \end{bmatrix} \tag{40}$$

$$\delta_q = \begin{bmatrix} 1 & 0 \end{bmatrix} \begin{bmatrix} \delta_q \\ \dot{\delta}_q \end{bmatrix}. \tag{41}$$

Here, $w_n = 300$ and $\zeta = 0.7$ nominally. Recall from Eq. 22 that the dynamic inversion controller accounts only for first-order dynamics with an internal model of the actuator bandwidth as in Fig. 5.

The desired closed loop bandwidth for the fast inner q loop is set to $\omega_q = 100$ radians per second. The desired closed loop bandwidth for the slow outer α loop is set to $\omega_\alpha = 50$ radians per second. The aerodynamic coefficients are scheduled across the relevant flight envelope for dynamic inversion. The resultant surface deflection

command δ_{d} is fed through the second-order actuator model to a fully nonlinear dynamic model of the projectile. Empirically, feeding back an internal model of the actuator dynamics requires the inclusion of a first-order filter in order to achieve acceptable performance. Finally, the sensitivity parameter σ in Eq. 38 is implemented as a linear function of the plant states for greater adaptation when the tracking error is significant. Scheduling σ does not impact the stability proof in the Appendix since we only require $\sigma > 0$.

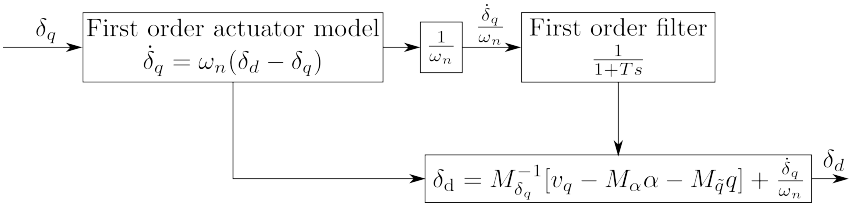

Fig. 5 Internal actuator model for the dynamic inversion control scheme

4.2 Nonlinear Simulation Analysis and Results

Both the proportional-integral (PI) and adaptive variants of the dynamic inversion controller are exercised in a flight simulation to evaluate performance. The simulation contains the equations of motion and a nonlinear aerodynamic model for the projectile along with a second-order actuator model as shown in Fig. 6. Notice the introduction of state disturbances at both the input and output of the nonlinear projectile dynamical model. The α-command generator is abstracted so as to consider both the PI and adaptive forms of that outer loop controller.

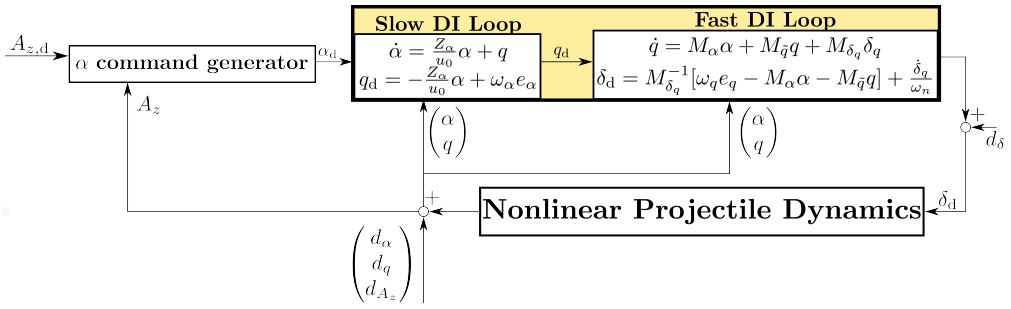

Fig. 6 Simulation overview

An A_z reference command of alternating 15 g positive and negative steps is chosen to exercise the controller, which is refined using a first-order filter with $\tau = 0.125$ to emulate commands from a guidance/navigation system. An initial error of -1°

in α is used at simulation start. The projectile flight is simulated for 10 s, starting from Mach 3.8 at sea level, with standard atmospheric conditions.

4.2.1 Nominal Simulation Results

Figure 7 plots the simulation results for both the PI and adaptive dynamic inversion controllers, with the A_z reference and result shown in a), α across the flight shown in b), the control deflection angle shown in c), q shown in d), and Mach number across the flight shown in e). The results from the simulation using the PI α-command generator variant are shown in blue, with the adaptive variant shown in orange. Both controller variants perform well in this simulation, and are able to accurately track the A_z reference command across a wide range of Mach, α flight conditions.

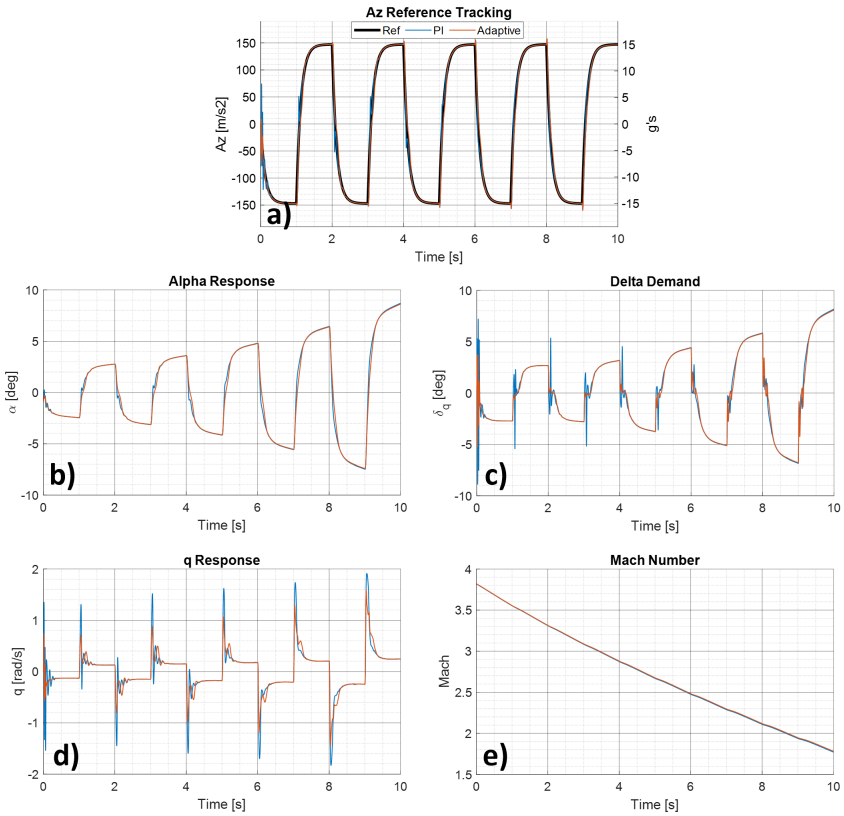

Fig. 7 Nonlinear simulation results for both the PI and adaptive variants of the dynamic inversion controller tracking a given A_z reference command

4.2.2 Results with Noise and Disturbances

Measurement noise and external disturbances are next included in the simulation to evaluate the controller performance under nonideal conditions. Band-limited white noise is added to 1) the feedback of q, α, and A_z to emulate noisy sensor mea-

surements and 2) the control deflection command signal to emulate external disturbances from atmospheric turbulence and wind gusts. As shown in Fig. 8, both controller variants perform well and are able to track the A_z reference command despite significant disturbances and degradation in the state measurements.

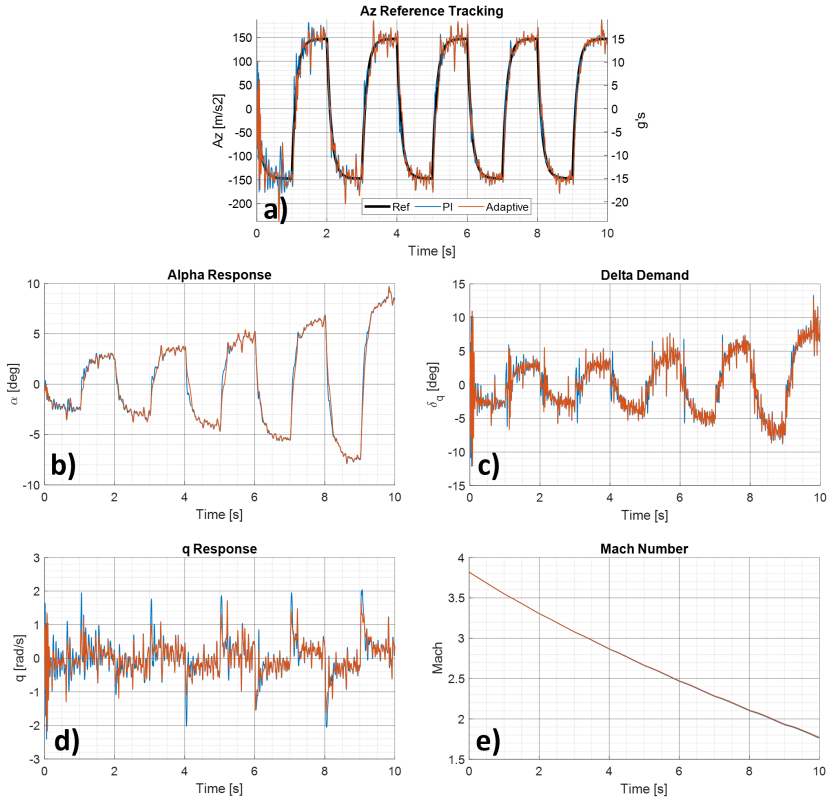

Fig. 8 Nonlinear simulation results with external disturbances and measurement noise for both the PI and adaptive variants of the dynamic inversion controller

4.2.3 Results with Scheduling Parameter Errors

Given the scheduled design of the controller, with gains that vary across the flight envelope, it is important to ensure the controller is robust to errors in estimation of the scheduling parameters. Additionally, this example application uses Mach and α as scheduling parameters, which are often difficult to estimate precisely from available onboard sensors. To investigate the sensitivity of the controller to uncertainties in these estimates, an analysis is performed such that Mach and α values within the controller are each scaled by $\pm 40\%$. This results in significant look-up table indexing errors for each scheduled controller gain and α measurement feedback errors in the α dynamic inversion loop, from Eq. 32. In this analysis, these errors are applied as a fixed scaling for each simulation run (as opposed to evolving errors throughout

the simulation). A follow-on analysis using more detailed estimation models with varying covariance and bias is recommended, but the magnitude of the static scaling errors is sufficient to give confidence in the overall robustness of the controller to schedule parameter errors.

Results for the PI variant dynamic inversion controller with $\pm 40\%$ estimation error in flight envelope parameters are shown in Fig. 9 in blue, along with the nominal simulation performance with perfect parameter estimates shown in orange for comparison. One particular case, with Mach underestimated by 40% and α overestimated by 40%, generated the most significant overshoots in A_z tracking. Overall, the controller performance is only degraded slightly, despite significant estimation errors.

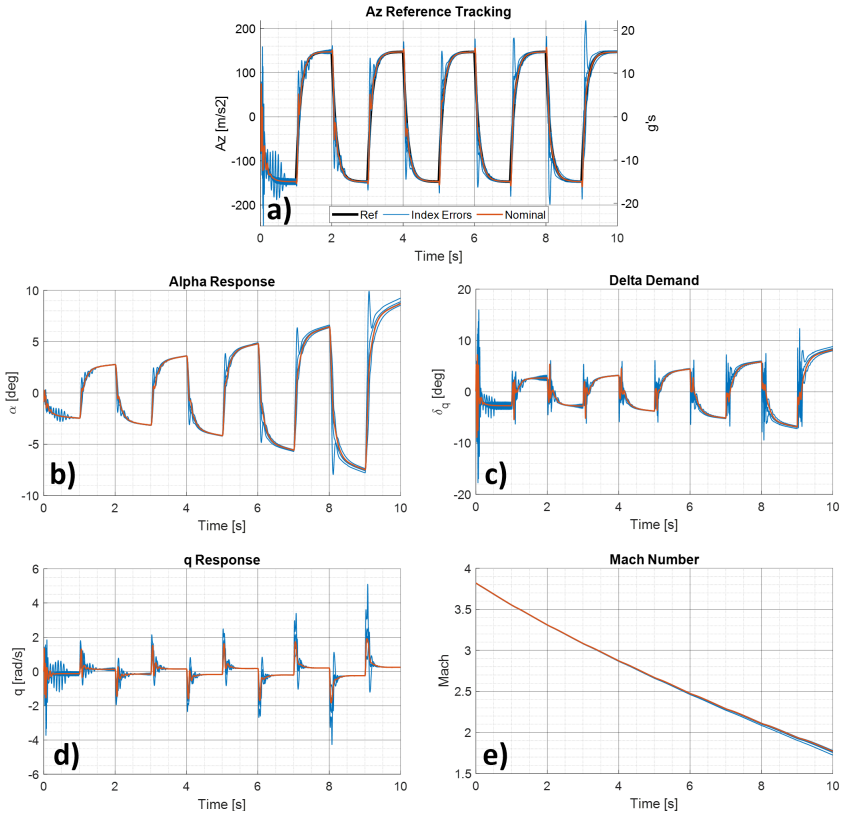

Fig. 9 Nonlinear simulation results for the PI dynamic inversion controller with $\pm 40\%$ estimation error in flight envelope parameters

Results for the adaptive controller variant with $\pm 40\%$ estimation error in flight envelope parameters are shown in Fig. 10 in blue, along with the nominal simulation results shown in orange for comparison. The adaptive regulator is able to adjust

to the parameter estimation errors within the first seconds of flight, and the subsequent tracking of the A_z reference command is nearly identical to the nominal case. Given these results, both controller variants appear robust to significant errors in scheduling parameter errors.

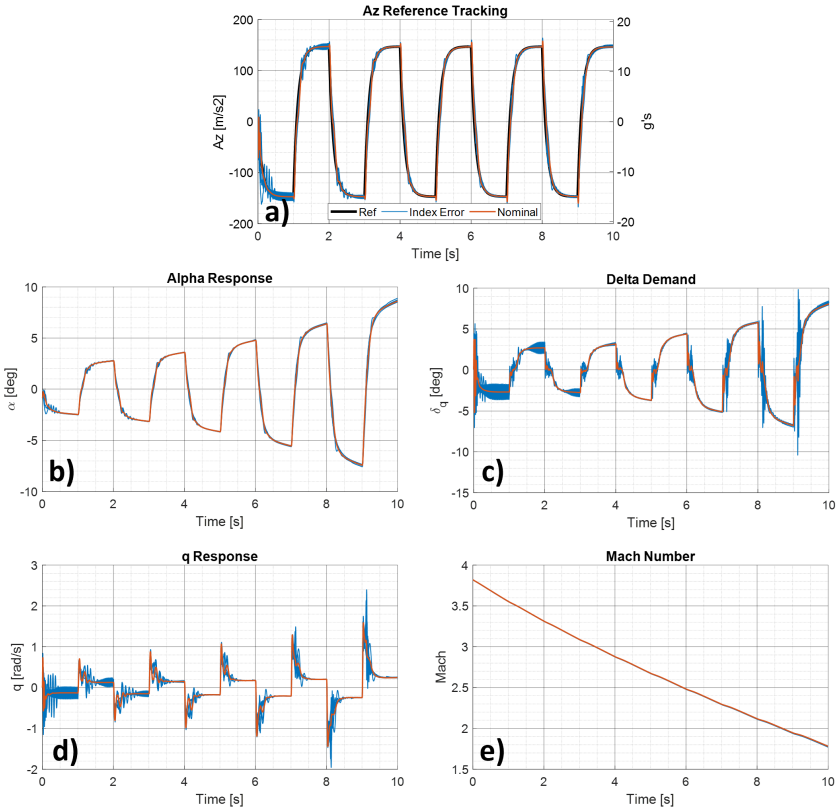

Fig. 10 Nonlinear simulation results for the adaptive dynamic inversion controller with $\pm 40\%$ estimation error in flight envelope parameters

4.2.4 Results with Model Parameter Errors

The dynamic inversion approach used for this controller relies heavily on the dynamic model of the system, given in Eq. 8, which is a simplified expression of the true dynamics, and comprises parameters and properties that are imperfectly known. The flight controller should be designed with robustness to this model error/uncertainty.

One source of model error is the linearization using the short-period approximation, which neglects aspects of the nonlinear dynamics in order to simplify the dynamic equations. In addition, the aerodynamic terms used within the model are obtained through the blending of multiple experimental and analytical techniques (compu-

tational fluid dynamics [CFD], wind tunnel, flight experiments, etc.); each has different strengths and limitations. This aerodynamic data fusion remains an area of active research, and the aerodynamic coefficients can have significant uncertainty, particularly in hypersonic flight regimes.

To explore the sensitivity of the controller to variations/errors in the projectile and actuator dynamic models, a Monte-Carlo (MC) analysis is performed using the nonlinear flight simulation. An uncertainty bound is set for each parameter within the dynamic models, as shown in Table 2. Uniform random draws are then made for each parameter within its respective uncertainty bounds, and the controller performance is evaluated to analyze the robustness to the specified model uncertainties.

Table 2 Dynamic model uncertainty bounds

Mass properties		**Environment parameters**		**Aerodynamic coefficients**		**Actuator properties**	
m	$\pm 10\%$	ρ	$\pm 20\%$	C_{Z_α}	$\pm 10\%$	ω_{n}	$[280 : 350]$ rad/s
I_y	$\pm 10\%$	V	$\pm 10\%$	C_{Z_δ}	$\pm 10\%$		
CG_x	± 0.1 cal			C_{m_α}	$\pm 20\%$ ± 0.1 cal		
				C_{m_δ}	$\pm 20\%$ ± 0.1 cal		
				C_{m_q}	$\pm 30\%$		

For this example, the projectile mass, m, and moment of inertia, I_y, are given an error bound of $\pm 10\%$ from their nominal values. The x-location of projectile CG is assumed to vary by ± 0.1 cal. The air density, ρ, is given an error of $\pm 20\%$, and the projectile velocity, V, is given a $\pm 10\%$ uncertainty. These combine together to define the uncertainty in the dynamic pressure, $Q = 1/2\rho V^2$.

The aerodynamic force coefficients $C_{Z_\alpha}, C_{Z_\delta}$ are both given an error bound of $\pm 10\%$, and the error in the damping coefficient, C_{m_q} is assumed to be $\pm 30\%$, as shown in Table 2. The aerodynamic moment coefficients are affected by the CG uncertainty, along with an assumed additional error bound of $\pm 20\%$. The effect of the CG shift on the aerodynamic moments is taken to be cumulative with the $\pm 20\%$ error.

The actuator response is also assumed to be uncertain, with a ω_{n} varying from 280 to 350 rad/s. This assumption captures uncertainties due to simplifications between the true dynamics and the second-order modeling approximation, as well as nonlinearities in the actuator response in the presence of significant hinge moments

due to aerodynamic forces on the control surfaces in high dynamic pressure flight conditions.

MC simulation results for the PI variant dynamic inversion controller are shown in Fig. 11 in blue, with the nominal simulation performance shown in orange for comparison. These results show some combinations of model errors result in degraded tracking for A_z commands corresponding to small α angles. The projectile in this example is unstable at these small α angles, and the combination of the unstable dynamics with the given uncertainty in the models results in undesired oscillations and overshoots for some of the model error combinations given in Table 2. Overall, the controller appears robust to a significant proportion of the defined model uncertainty space, particularly when controlling at higher angles of attack.

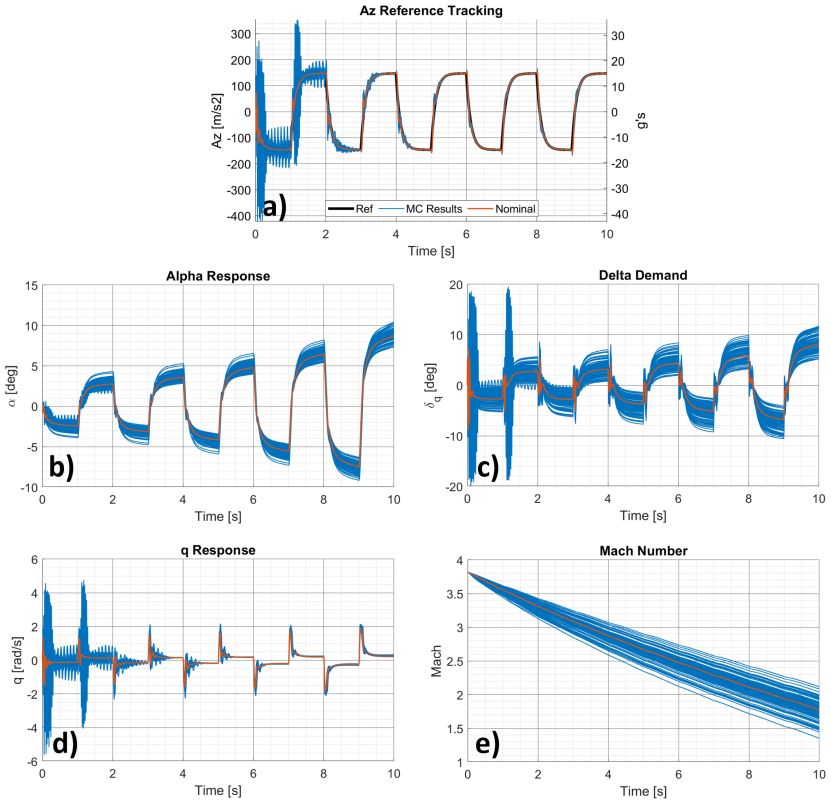

Fig. 11 MC analysis results for the PI dynamic inversion controller with model errors

MC simulation results for the adaptive variant dynamic inversion controller are shown in Fig. 12 in blue, with the nominal simulation performance shown in orange for comparison. The adaptive regulator is able to adjust to the modeling errors within the first seconds of flight, and the subsequent tracking of the A_z reference

command is nearly identical to the nominal case (even at low-α angles) despite the significant modeling errors.

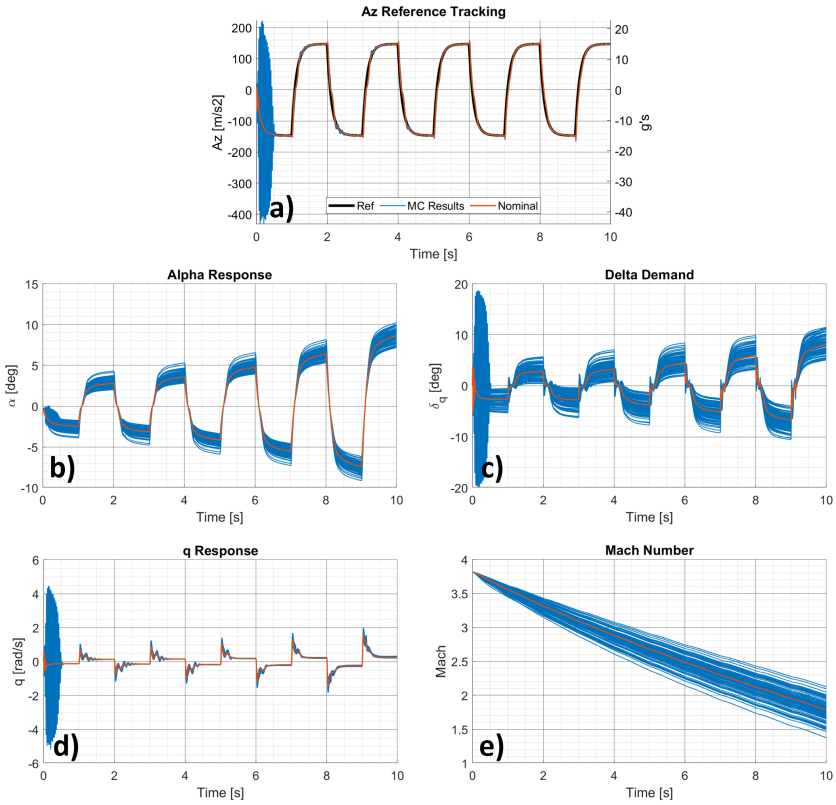

Fig. 12 MC analysis results for the adaptive dynamic inversion controller with model errors

5. Conclusions

A scheduled, linear dynamic inversion controller was described for the autopilot of a high-speed projectile. The dynamic inversion was applied to the short-period dynamics of the projectile, and a time scale separation scheme was employed for robustness. Notably, an internal model of the actuator dynamics was included to account for actuator bandwidth limits.

The nonminimum phase acceleration dynamics of this tail-controlled projectile cannot be safely inverted, so an outer loop was used to convert acceleration commands into α commands. Two variants of this outer loop were investigated, one using a conventional PI approach and another using an adaptive regulator.

Both variants of the controller were exercised using nonlinear simulation and showed significant robustness to measurement noise, external disturbances, scheduling pa-

rameter errors and modeling errors, with the adaptive variant providing marginally improved tracking performance in some circumstances. The schemes presented here offer a compelling control architecture when the plant dynamics are well characterized. The dynamic inversion approach is particularly recommended as a nominal architecture that may be quickly implemented for comparison with other schemes or initial airframe testing.

6. References

1. Gruenwald BC, Bryson J. A gain-scheduled approach for the control of a high-speed guided projectile. AIAA Scitech 2022 Forum; 2022 Jan. Paper No.: AIAA 2022-0612.

2. Bryson J, Gruenwald BC. Automated gain-scheduling approach for three-loop autopilot. DEVCOM Army Research Laboratory (US); 2022 Sep. Report No.: ARL-TR-9564.

3. Tipàn S, Theodoulis S, Thai S, Proff M. Nonlinear dynamic inversion flight control design for guided projectiles. Journal of Guidance, Control, and Dynamics. 2020;43(5):975–980.

4. Thai S, Theodoulis S, Roos C, Biannic JM. Robust design for the roll-channel autopilot of a canard-guided dual-spin projectile. IFAC-PapersOnLine. 2019;52(12):232–237.

5. Lee HP, Clemens JW, Youssef HM. Dynamic inversion flight control design for aircraft with non-minimum phase response. Aerospace Technology Conference and Exposition; 2011 Oct. SAE International. Paper No.: 2011-01-2617.

6. Kutluay KT, Yavrucuk I. Dynamic inversion based control of a missile with L1 adaptive control augmentation. 2010 IEEE International Symposium on Intelligent Control; 2010 Sep. p. 2374–2379.

7. Menon P, Iragavarapu V, Ohlmeyer E. Nonlinear missile autopilot design using time-scale separation. Guidance, Navigation, and Control Conference; 1997 Aug. Paper No.: AIAA-97-3765.

8. Harris J, Elliott CM, Tallant GS. Stability and performance robustness of an L1 adaptive dynamic inversion flight control system. AIAA Scitech 2019 Forum; 2019 Jan. Paper No.: AIAA 2019-0141.

9. Siwakosit W, Snell S, Hess R. Robust flight control design with handling qualities constraints using scheduled linear dynamic inversion and loop-shaping. IEEE Transactions on Control Systems Technology. 2000;8(3):483–494.

10. Snell A. Decoupling control design with applications to flight. Journal of Guidance, Control, and Dynamics. 1998;21(4):647–655.

11. Snell A, Hess R, Siwakosit W. Flight control design using scheduled linear dynamic inversion and quantitative feedback theory. Guidance, Navigation, and Control Conference and Exhibit; 1998 Aug. Paper No.: AIAA-98-4421.

12. Steffensen R, Steinert A, Smeur EJJ. Non-linear dynamic inversion with actuator dynamics: an incremental control perspective. arXiv preprint. 2022;arXiv:2201.09805.

13. Lombaerts T, Kaneshige J, Schuet S, Aponso BL, Shish KH, Hardy G. Dynamic inversion based full envelope flight control for an eVTOL vehicle using a unified framework. AIAA Scitech 2020 Forum; 2020 Jan. Paper No.: AIAA 2020-1619.

14. Reiner J, Balas GJ, Garrard WL. Flight control design using robust dynamic inversion and time-scale separation. Automatica. 1996;32(11):1493–1504.

15. Vasile JD, Bryson J, Gruenwald BC, Fairfax L, Strohm L, Fresconi F. A multidisciplinary approach to design long range guided projectiles. AIAA Scitech 2020 Forum; 2020 Jan. Paper No.: AIAA 2020-1993.

16. Bryson J, Vasile JD, Gruenwald BC, Saju J, Fresconi F. Modeling and flight dynamics of a projectile with nonlinear, roll-dependent aerodynamics. AIAA Scitech 2021 Forum; 2021 Jan. Paper No.: AIAA 2021-0823.

17. Burchett BT, Vasile JD, Bryson J. Combining sparse and dense databases to form a robust aerodynamic model for a long-range, high-speed projectile. AIAA Scitech 2022 Forum; 2022 Jan. Paper No.: AIAA 2022-0419.

18. Bryson J, Vasile JD, Gruenwald BC, Fresconi F. Control surface design analysis and actuation requirements development for munitions. AIAA Scitech 2020 Forum; 2020 Jan. Paper No.: AIAA 2020-0020.

19. Chen WH. Nonlinear disturbance observer-enhanced dynamic inversion control of missiles. Journal of Guidance, Control, and Dynamics. 2003;26(1):161–166.

20. Valasek J, Ito D, Ward D. Robust dynamic inversion controller design and analysis for the X-38. AIAA Guidance, Navigation, and Control Conference and Exhibit; 2001 Aug. Paper No.: AIAA 2001-4380.

Appendix. Stability Proof

Our model of the aerodynamic coefficient $\bar{Z}_\alpha^{-1}$ may have significant parametric uncertainty and so not be equal to the true value of the coefficient Z_α^{-1}. We wish to implement an adaptive scheme to correct $\bar{Z}_\alpha^{-1}$ online. Notice, this parametric error introduces an error in α

$$e_\alpha = \hat{\alpha} - \alpha \tag{A-1}$$

which has dynamics

$$\begin{aligned}
\dot{e}_\alpha &= \dot{\hat{\alpha}} - \dot{\alpha} \\
&= -\omega_\alpha \hat{\alpha} - \omega_\alpha \bar{Z}_\alpha^{-1} A_{z,\text{CMD}} + \omega_\alpha \alpha + \omega_\alpha Z_\alpha^{-1} A_{z,\text{CMD}} \\
&= -\omega_\alpha e_\alpha - \omega_\alpha \bar{Z}_\alpha^{-1} A_{z,\text{CMD}} + \omega_\alpha Z_\alpha^{-1} A_{z,\text{CMD}}.
\end{aligned} \tag{A-2}$$

Suppose $\bar{Z}_\alpha^{-1} \equiv Z_\alpha^{-1} + \Delta Z_\alpha^{-1}$. This yields

$$\begin{aligned}
\dot{e}_\alpha &= -\omega_\alpha e_\alpha - \omega_\alpha Z_\alpha^{-1} A_{z,\text{CMD}} + \omega_\alpha \Delta Z_\alpha^{-1} A_{z,\text{CMD}} + \omega_\alpha Z_\alpha^{-1} A_{z,\text{CMD}} \\
&= -\omega_\alpha e_\alpha + \omega_\alpha \underbrace{\Delta Z_\alpha^{-1} A_{z,\text{CMD}}}_{w} \\
&= -\omega_\alpha e_\alpha + \omega_\alpha w \\
&= A_c e_\alpha + B w.
\end{aligned} \tag{A-3}$$

Assign the output dynamics

$$\begin{aligned}
e_y = e_{A_z} &= A_{z,\text{CMD}} - A_z \\
&= Z_\alpha^{-1} e_\alpha.
\end{aligned} \tag{A-4}$$

The stability proof that follows relies heavily on the notion of almost strict dissipativity (ASD). The system dynamics

$$\begin{aligned}
\dot{x} &= Ax + Bu \\
y &= Cx
\end{aligned} \tag{A-5}$$

are ASD if they satisfy the Kalman-Yakubovich conditions:

$$\begin{aligned}
A_c^* P + P A_c &= -Q \\
PB &= C^*
\end{aligned} \tag{A-6}$$

for some positive definite matrices P and Q. A_c^* denotes the conjugate transpose of A_c. The matrix $A_c = A + BGC$ may stabilize A with a stable gain matrix G and is equivalent to the closed loop matrix for the system in Eq. A-5 under the feedback law $u = Gy$. The ASD property is equivalent to the open loop system having a positive definite high-frequency gain and stable minimum phase transmission zeros.[1]

With the error dynamics in Eq. A-3, assign the following Lyapunov function to the e_α

$$V_1(e_\alpha) = \frac{1}{2} e_\alpha^* P e_\alpha \tag{A-7}$$

where P comes from the ASD condition $AP + PA = -Q$ and $PB = C^*$. This function has the Lie derivative

$$\begin{aligned}
\dot{V}_1 &\equiv e_\alpha^* P \dot{e}_\alpha \\
&= e_\alpha^* P (A e_\alpha + B w) \\
&= e_\alpha^* P A e_\alpha + e_\alpha^* P B w \\
&= -\frac{1}{2} e_\alpha^* Q e_\alpha + e_\alpha^* P B w \\
&= -\frac{1}{2} e_\alpha^* Q e_\alpha + e_\alpha^* C^* w \\
&= -\frac{1}{2} e_\alpha^* Q e_\alpha + e_{A_z}^* w \\
&= -\frac{1}{2} e_\alpha^* Q e_\alpha + (e_{A_z}, w).
\end{aligned} \tag{A-8}$$

The adaptive gain has the Lyapunov function

$$V_2(\Delta Z_\alpha^{-1}) \equiv \frac{1}{2} \text{tr}(\Delta Z_\alpha^{-1} \sigma^{-1} \Delta Z_\alpha^{-1^*}). \tag{A-9}$$

Accordingly,

$$\dot{V}_2(\Delta Z_\alpha^{-1}) = \text{tr}(\Delta \dot{Z}_\alpha^{-1} \sigma^{-1} \Delta Z_\alpha^{-1^*}). \tag{A-10}$$

[1] Balas M, Fuentes R. A non-orthogonal projection approach to characterization of almost positive real systems with an application to adaptive control. Proceedings of the 2004 American Control Conference; 2004 July; Vol. 2. IEEE; p. 1911–1916.

Notice, by assigning the update law

$$\Delta \dot{Z}_{\alpha}^{-1} \equiv -e_{A_z} A_{z,\text{CMD}}^{*} \sigma, \sigma > 0, \tag{A-11}$$

yields

$$\begin{aligned} \dot{V}_2(\Delta Z_{\alpha}^{-1}) &= \text{tr}(-e_{A_z} A_{z,\text{CMD}}^{*} \sigma \sigma^{-1} \Delta Z_{\alpha}^{-1^{*}}) \\ &= -\text{tr}(e_{A_z} \underbrace{A_{z,\text{CMD}}^{*} \Delta Z_{\alpha}^{-1^{*}}}_{w^{*}}) \\ &= -(e_{A_z}, w). \end{aligned} \tag{A-12}$$

Therefore, the system composite Lyapunov function is

$$\begin{aligned} V(e_{\alpha}, \Delta Z_{\alpha}^{-1}) &= V_1 + V_2 \\ &= -\frac{1}{2} e_{\alpha}^{*} Q e_{\alpha} + (e_{A_z}, w) - (e_{A_z}, w) \\ &= -\frac{1}{2} e_{\alpha}^{*} Q e_{\alpha}, \end{aligned} \tag{A-13}$$

which bounds the trajectory $e_{\alpha}(t)$ and ΔZ_{α}.

Now consider the function

$$W(e_{\alpha}) \equiv \frac{1}{2} \lambda_{\min}(Q) ||e_{\alpha}||^2 \tag{A-14}$$

and take the time derivative yielding

$$|\dot{W}(e_{\alpha})| = \lambda_{\min}(Q) |e_{\alpha}^{*} \dot{e}_{\alpha}|. \tag{A-15}$$

Substitute $\dot{e}_{\alpha}$ from Eq. A-3 to see that

$$|\dot{W}(e_{\alpha})| = \lambda_{\min}(Q) \left| e_{\alpha}^{*} \left(A_c e_{\alpha} + B \Delta Z_{\alpha}^{-1} A_{z,\text{CMD}} \right) \right|. \tag{A-16}$$

While Eq. A-13 bounds e_{α} and ΔZ_{α}^{-1}, it does not bound $A_{z,\text{CMD}}$. We employ the assumption that as a property of the plant, the command $A_{z,\text{CMD}}$ is bounded. Given this, the derivative of Eq. A-14 is also bounded, and $W(e_{\alpha})$ is uniformly continuous by the mean value theorem. Finally, by Barbalat's lemma[2], $e_{\alpha}(t) \to 0$ as $t \to \infty$.

[2]Khalil HK. Nonlinear systems. Prentice Hall; 2002.

List of Symbols, Abbreviations, and Acronyms

CG	center-of-gravity
MC	Monte Carlo
PI	proportional-integral
ASD	almost strictly dissipativity

MATHEMATICAL SYMBOLS:

$\mathbb{C}^n$	set of $n \times 1$ complex column vectors
$\equiv$	equality by definition

MATHEMATICAL OPERATORS:

$(\dot{\ })$	denotes the time-derivative
$(\vec{\ })$	denotes a vector
$(\cdot)^{\mathrm{T}}$	denotes the transpose operator
$(\cdot)^{\dagger}$	denotes the pseudo-inverse operator
$(\cdot)^{-1}$	denotes the inverse operator

1 (PDF)	DEFENSE TECHNICAL INFORMATION CTR DTIC OCA
1 (PDF)	DEVCOM ARL FCDD RLB CI TECH LIB
18 (PDF)	DEVCOM ARL FCDD RLA CL F E FRESCONI FCDD RLA W T SHEPPARD FCDD RLA WD J T BRYSON B C GRUENWALD L STROHM B BURCHETT I CELMINS J DESPIRITO L FAIRFAX J PAUL J D VASILE FCDD RLA WA N TRIVEDI FCDD RLA WB J SADLER FCDD RLA WC M MINNICINO FCDD RLA WE M ILG B TOPPER J MALEY FCDD RLA WF E RIGAS